The Astronomical Journal, 120:2101–2113, 2000 October

THE PUZZLE OF HD 104994 (WR 46)[1]

Sergey V. Marchenko
Département de Physique, Université de Montréal, C.P. 6128, Succursale Centre-Ville, Montreal, QC H3C 3J7, Canada; and Observatoire du Mont Mégantic; sergey@astro.umontreal.ca

Julia Arias[2] and Rodolfo Barbá[2,3]
Facultad de Ciencias Astronómicas y Geofísicas, Universidad Nacional de la Plata, Paseo del Bosque, 1900 La Plata, Argentina; jarias@fcaglp.fcaglp.unlp.edu.ar, rbarba@fcaglp.fcaglp.unlp.edu.ar

Luis Balona
South African Astronomical Observatory, P.O. Box 9, Observatory 7935, South Africa; lab@maia.saao.ac.za

Anthony F. J. Moffat[4]
Département de Physique, Université de Montréal, C.P. 6128, Succursale Centre-Ville, Montreal, QC H3C 3J7, Canada; and Observatoire du Mont Mégantic; moffat@astro.umontreal.ca

Virpi S. Niemela[2,5]
Facultad de Ciencias Astronómicas y Geofísicas, Universidad Nacional de la Plata, Paseo del Bosque, 1900 La Plata, Argentina; virpi@fcaglp.fcaglp.unlp.edu.ar

Michael M. Shara[2]
Department of Astrophysics, Division of Physical Sciences, American Museum of Natural History, Central Park West at 79th Street, New York, NY 10024-5192; mshara@amnh.org

and

Christiaan Sterken[6]
Vakgroep Natuurkunde, Vrije Universiteit Brussel, Pleinlaan 2, B-1050 Brussel, Belgium; csterken@vub.ac.be

Received 2000 May 17; accepted 2000 June 22

ABSTRACT

Intense coordinated spectroscopic and photometric monitoring of the suspected Wolf-Rayet binary WR 46 in 1999 reveals clear periodic variations, $P = 0.329 \pm 0.013$ days, in the radial velocities of the emission lines of highest ionization potential, O VI and N V, found deepest in the Wolf-Rayet wind and thus least likely to be perturbed by a companion. These are accompanied by coherent variability in the profiles of lines with lower ionization/excitation potential and in the continuum flux. Most probably originating from orbital motion of the Wolf-Rayet component of the binary, this periodic radial velocity signal disappears from time to time, thus creating a puzzle yet to be solved. We show that the entangled patterns of the line profile variability are mainly governed by transitions between high and low states of the system's continuum flux.

Key words: stars: individual (WR 46) — stars: variables: general — stars: Wolf-Rayet

1. INTRODUCTION

The Wolf-Rayet (W-R) star HD 104994 (DI Cru, WR 46) is a rather unique object in the Catalogue of Galactic Wolf-Rayet Stars (van der Hucht et al. 1981), demonstrating a complex superposition of large-amplitude, long-term (months, years) photometric variations (Marchenko et al. 1998b; Veen et al. 2000) and extremely short term (hours) photometric and spectral changes. These are fitted with sometimes contradictory periods (see Veen et al. 2000 for an up-to-date description of the observational history). The presence of relatively strong O VI lines in the optical region (for a sample optical spectrum, see Niemela, Barbá, & Shara 1995) is a rather unusual feature for a nitrogen-sequence W-R star, as those lines usually appear in the spectra of presumably hotter and more evolved stars of the oxygen-rich WO sequence (Kingsburgh & Barlow 1995). Niemela et al. (1995) were the first to note the spectral similarity of WR 46 and the class of supersoft X-ray sources, an idea recently promoted by Steiner & Diaz (1998), ascribing to WR 46 membership in a newly established group of low-mass variables, the "V Sagittae stars." This classification was primarily based on the presence of strong emission from high-ionization species of O VI and N V along with specific variability patterns, namely, the long-term (years, probably aperiodic) and short-term (hours, periodic) optical brightness variations accompanied by short-term periodic variability of radial velocities (RVs). If WR 46 is a member of the "V Sagittae" group, then the optical emission spectrum should arise in an accretion disk, which only mimics the general appearance of a typical W-R spectrum. On the other hand, WR 46 was classified as a Population I WN3 object by means of ultraviolet-to-infrared fitting of its spectrum with models of a standard W-R atmosphere (Schmutz, Hamann, & Wessolowski 1989; Crowther, Smith, & Hillier 1995; Hamann & Koesterke 1998), with a note from Crowther et al. that the chemical composition of WR 46 is rather peculiar. Intrigued by the uncertainty in the origin of the WR 46 spectrum and, specifically, by its unusual variability patterns, we decided to organize coordinated observations of the star. Recently we learned that the system was experiencing some gradual brightening during our 1999 campaign (A. Jones 1999, private communication; Veen et al. 2000).

[1] Based in part on observations obtained at the European Southern Observatory, La Silla, Chile (ESO program 62.H-0110).
[2] Visiting Astronomer, CASLEO, San Juan, Argentina.
[3] Member of Carrera del Investigador, CONICET, Argentina.
[4] Killam Research Fellow of the Canada Council for the Arts.
[5] Member of Carrera del Investigador, CICBA, Argentina.
[6] Belgian Fund for Scientific Research (FWO).

TABLE 1

RADIAL VELOCITY MEASUREMENTS

HJD (2,450,000+)	RV(He II + N V) (km s^{-1})	σ(RV) (km s^{-1})	RV(O VI) (km s^{-1})	RV(N V λ4944) (km s^{-1})
1,261.6824.....	−16	6	−35	−86
1,261.6937.....	−20	5	−14	−83
1,261.7067.....	−39	7	−29	−87
1,261.7184.....	−27	5	−28	−87
1,261.7314.....	−57	10	−49	−101

NOTE.—Table 1 is presented in its entirety in the electronic edition of the Astronomical Journal. A portion is shown here for guidance regarding its form and content.

2. OBSERVATIONS

We organized a multisite, intense monitoring campaign of WR 46, following the star spectroscopically from the Complejo Astronómico El Leoncito (CASLEO),[7] San Juan, Argentina, during seven contiguous nights in 1999 March, using the Cassegrain REOSC spectrograph attached to the 2.15 m telescope. The combination of a 600 line mm^{-1} grating and a Tektronix 1024 × 1024 CCD (24 × 24 μm pixel size) provided spectral coverage of 3695–5385 Å with spectral resolution of ~4.2–5.0 Å (2.5–3.0 pixels) for a typical 15 minute exposure, reaching signal-to-noise ratio $\langle S/N \rangle = 230 \pm 50$ at $\lambda \sim 4800$ Å (continuum). The spectra were processed using IRAF.[8] For wavelength calibration we acquired HeAr lamp spectra before and after stellar exposures, bringing the internal errors of calibration down to $\lesssim$0.1 pixels ($\pm$10 km s^{-1}). The final wavelength adjustment was performed by measuring the RV of interstellar absorption features: Ca II H and K lines in all spectra, and diffuse absorption features at 4501 and 4762 Å in the spectra with S/N > 200. Then all the deviating spectra were shifted to the mean positions of the interstellar lines (17 out of 134 available spectra, an average correction by $\pm$75 km s^{-1}) to account for systematic velocity shifts across the whole spectrum, which are most likely due to an instrumental glitch, as we observed similar sporadic shifts during previous runs. We found the corrected spectra to form short sequences, one to four spectra for a given night with the exception of night 5, when no deviations were registered. The instrumental glitches happened to occur at the end of a night. As 14 out of the 17 corrected spectra were redshifted, we may conclude that, overall, applying the correction tends to reduce the amplitude of the observed RV variations. A journal of spectroscopic observations and measured RVs is given in Table 1.

In 1999 February–March, WR 46 was also followed photometrically from the South African Astronomical Observatory using a single-channel photometer attached to the 0.5 m telescope. With *UBVRI* broadband filters and HD 103779 as a comparison star, a typical rms scatter of 0.005 mag in V and in the color indexes was achieved. We list the SAAO observations in Table 2. Additional, high-precision Strömgren photometry in b (dominated by strong He II λ4686 emission over the continuum flux) and y (continuum dominated) was obtained at ESO using the Dutch 90 cm telescope equipped with a CCD camera (512 × 512 pixels, ESO No. 33 detector). Differential photometry on the frames was performed with respect to two comparison stars, C_1 = GSC 8978443 and a nearby check star C_2 located 7″ north and 26″ east of C_1. This intense photometric monitoring (Table 3) overlapped with the spec-

[7] CASLEO is operated under agreement between CONICET, SECYT, and the national universities of La Plata, Córdoba, and San Juan, Argentina

[8] IRAF is distributed by the National Optical Astronomy Observatories, operated by the Association of Universities for Research in Astronomy, Inc., under cooperative agreement with the National Science Foundation.

TABLE 2

PHOTOMETRY OF WR 46 OBTAINED AT SAAO

HJD (2,450,000+)	V	$B-V$	$U-B$	$V-R$	$V-I$
1233.4015.....	10.891	−0.023	−0.817	0.145	0.268
1233.4075.....	10.893	−0.025	−0.808	0.142	0.286
1233.6123.....	10.824	−0.005	−0.808	0.140	0.289
1233.6177.....	10.829	−0.013	−0.805	0.148	0.297
1234.4061.....	10.900	−0.023	−0.825	0.143	0.274

NOTE.—Table 2 is presented in its entirety in the electronic edition of the Astronomical Journal. A portion is shown here for guidance regarding its form and content.

TABLE 3

PHOTOMETRY OF WR 46 OBTAINED AT ESO

HJD (2,450,000+)	WR − C_1	$C_1 - C_2$	HJD (2,450,000+)	WR − C_1	$C_1 - C_2$
	b			y	
1,179.8161.....	−2.515	−0.440	1,179.7537.....	−1.440	−0.920
1,181.8043.....	−2.414	−0.454	1,179.8142.....	−1.420	−0.915
1,182.8274.....	−2.519	−0.452	1,181.8021.....	−1.385	−0.918
1,182.8369.....	−2.525	−0.451	1,182.8258.....	−1.422	−0.920

NOTE.—Table 3 is presented in its entirety in the electronic edition of the Astronomical Journal. A portion is shown here for guidance regarding its form and content.

troscopic observations, providing a unique possibility to disentangle the continuum and line profile variations.

3. RESULTS

Our first goal was to confirm the periodic RV and light variations revealed in previous studies. We measured the RVs of the prominent emission lines by Voigt profile fitting to the individual profiles, thus treating the N v $\lambda\lambda$4943, 4945 blend as a single line; deblending the O vi $\lambda\lambda$3811, 3834 doublet with subsequent averaging of the measured RVs; cross-correlating the relevant segments of individual spectra with the seven-night mean spectrum to obtain the RVs of the N v + He ii $\lambda\lambda$4603–4686 complex (Table 1). We group the N v $\lambda\lambda$4603, 4619 doublet and the dominating He ii λ4686 emission line together, as they show a remarkably similar response to both periodic and seemingly stochastic perturbations. Indeed, measuring the line fluxes within fixed spectral regions in the rectified WR 46 spectra, we find a nearly perfect correlation, $r = 0.94 \pm 0.02$, between the variability of the N v and He ii emission fluxes. Moreover, their corresponding RVs [measured as centroids of the upper parts of the profiles, $(0.5–1.0)I_{max}$, to avoid blending] also show a high degree of correlation, $r = 0.94$. The Pickering He ii lines show similar RV and equivalent width (EW) behavior as the N v + He ii complex.

Searching for periodic variability with the CLEAN algorithm, developed by Roberts, Lehár, & Dreher (1987), we find a clear signal with $P = 0.329 \pm 0.013$ days (Fig. 1, *top two panels*) in the O vi lines, with the N v profile closely following the RV(O vi) variations with somewhat smaller amplitude (Fig. 2, *left*). This period is compatible with the $P = 0.31$ day periodicity discovered by Niemela et al. (1995) in their 1993–1994 spectra of WR 46. However, in 1999 we observed a far smaller amplitude in RV variations. Folding our RV data with the 1 day aliases of the principal 0.33 day periodicity, we obtain a radial velocity curve of somewhat lower quality for $P = 0.49$ days and significantly lower quality for $P = 0.25$ days, which prompts us to decide in favor of the $P = 0.329$ day period.

Both the EW of the emission lines of relatively low ionization potential and the underlying continuum follow the 0.33 day period (Fig. 1, *bottom two panels*), though in rather different ways. Note that the EWs shown in Figure 1 were measured relative to the variable continuum level. Hence, as shown, the EW minimum in N v and He ii + N v around $\phi = 0.75$ appears slightly shallower than it would be if the variable continuum flux were taken into account. The simplicity of this picture is lost while attempting to trace the 0.33 day periodic signal in the RVs of the N v + He ii $\lambda\lambda$4603–4686 complex, as there the RVs show significant phase lag, which varies with the ever-changing level of the absolute flux of the system (Fig. 2, *left*; see below). Additional complications come from the discovery that (1) the EW of the O vi doublet can be regarded as constant (Fig. 1, *bottom*) when taking into account the variable continuum level, (2) the value of the systemic velocity is "epoch" dependent (more correctly, orbital cycle–dependent; Fig. 1, *top*), and (3) the periodic RV signal disappears from time to time (Fig. 1, *second from top*).

The last, rather astonishing, finding prompts a split of the spectroscopic data into two clear categories of RV variability: the "moving" case (nights 3, 4, 6, 7; Fig. 1, *second from top, open circles*) and the "nonmoving" case (nights 1, 2, 5; Fig. 1, *second from top, filled circles*). However, detailed analysis of the spectral variability patterns in conjunction with the variable stellar flux forces us to subdivide the data even further, defining a high state (substantial brightening in the continuum: nights 3, 4; cf. Fig. 2, *right*) and a low state (the remainder of the data).

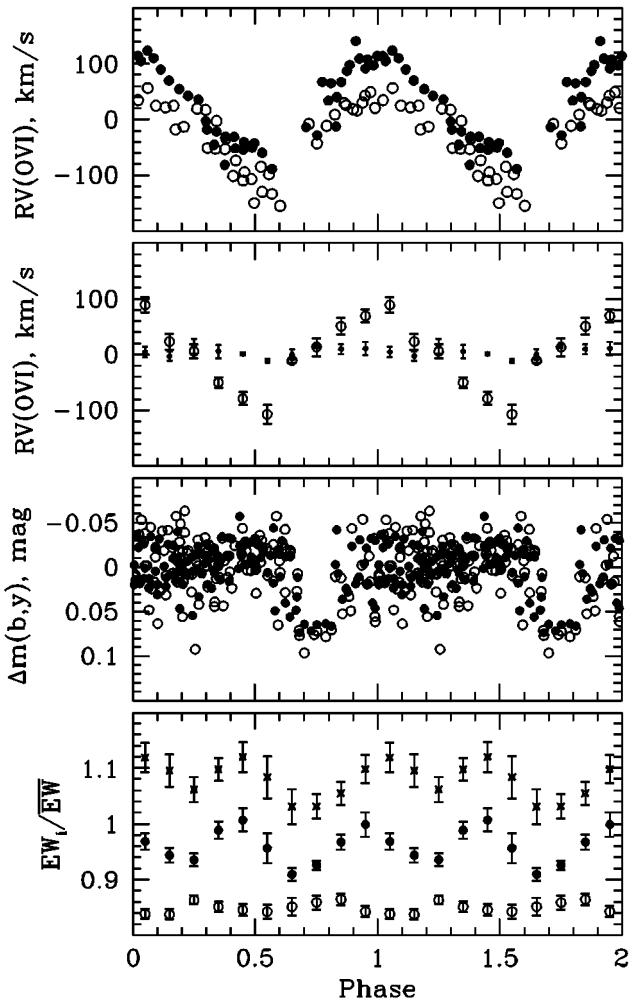

FIG. 1.—*Top*: Radial velocities of the O vi 3811 Å line folded with the 0.329 day period, with filled circles denoting the first part of the "moving" subset (38 spectra from nights 3 and 4) and open circles marking the second part of the moving subset (38 spectra from nights 6 and 7). We choose HJD 2,451,261.4 ± 0.05 days as a tentative zero-phase date based on the time of maximum RV. *Second from top*: RV(O vi) for the moving case grouped into 0.1 phase bins with corresponding 2 σ error bars (*open circles*; 76 spectra from nights 3, 4, 6, 7), and the same but for the "nonmoving" case (*filled circles*; 58 spectra from nights 1, 2, 5). *Second from bottom*: The Strömgren *y* (*filled circles*) and *b* (*open circles*) photometry folded with the 0.329 day period. The nightly mean values were subtracted from the original data to reduce the impact of long-term variability. The photometric error bars, 2 $\sigma(y) = 0.007$ mag, would be comparable to the symbol size if plotted. *Bottom*: Equivalent widths of He ii λ4686 + N v $\lambda\lambda$4603, 4619 blend (*crosses*), N v λ4944 (*filled circles*), and O vi (sum of the two components of the doublet; *open circles*), all folded with the 0.329 day period and plotted with 2 σ error bars. To compare the amplitudes of the EW variability, we apply the same relative scales to the measured lines, slightly offsetting the plots for clarity.

Measuring the RV variations of the He ii + N v complex in the available WR 46 spectra taken in 1993 (Niemela et al. 1995: basically the same instrumental setup as in 1999, except the 2.7 times higher spectral resolution; comparable exposure times, but low S/N $\lesssim$ 30 for the 1993 data), we find some indication of an apparent ceasing of the orbital

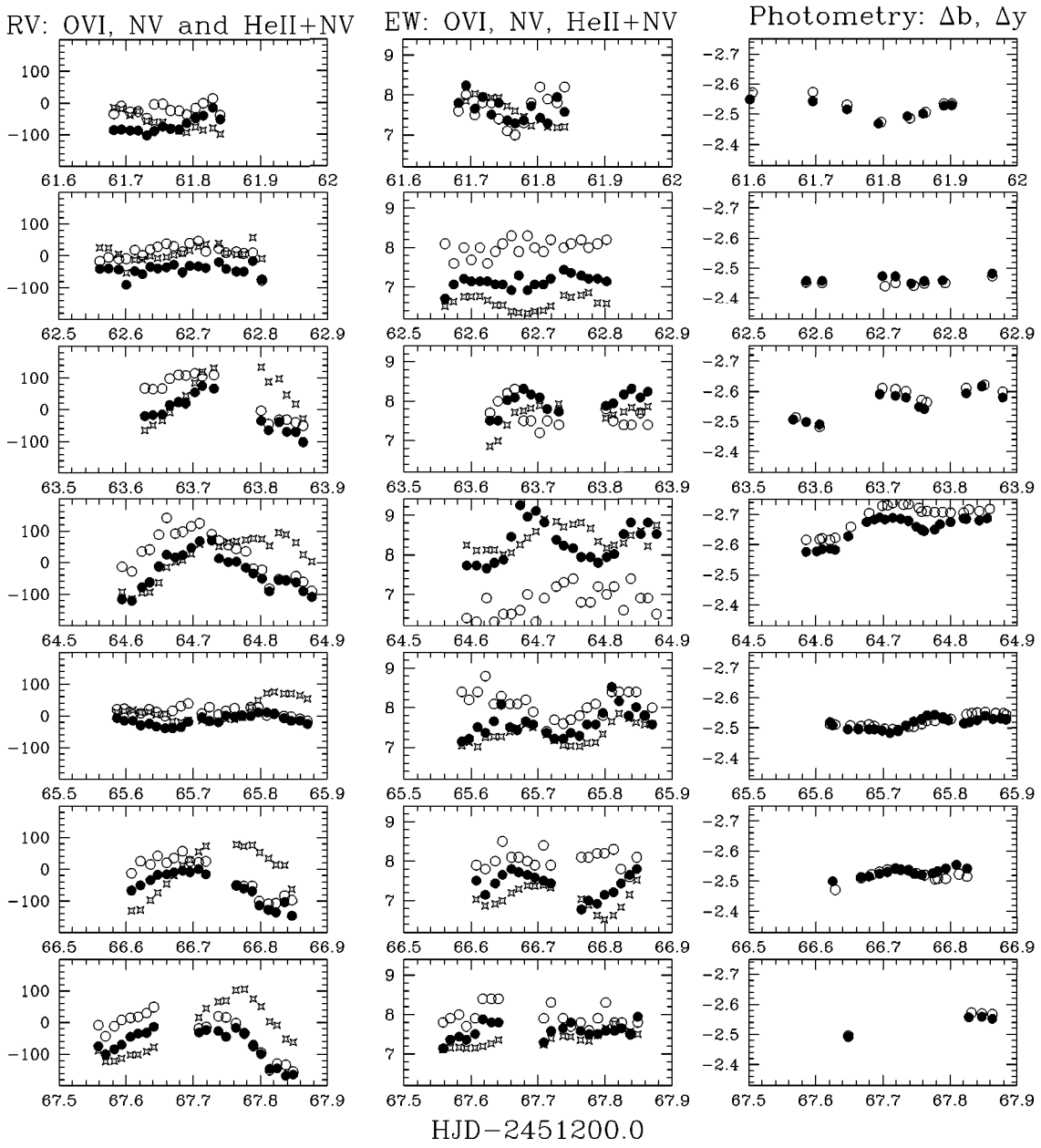

FIG. 2.—Simultaneous spectroscopy and photometry of WR 46 with contiguous nights plotted from top (mean HJD 2,451,261.5; night 1) to bottom (mean HJD 2,451,267.5; night 7). *Left*: Radial velocities, in kilometers per second. *Open circles*, O VI λλ3811, 3834; *stars*, N V λλ4603, 4619 + He II λ4686; *filled circles*, N V λ4944. *Middle*: Equivalent widths, in angstroms, for the O VI feature, with the EWs of two other lines scaled and shifted accordingly to fit the figure limits. *Open circles*, O VI λλ3811, 3834; *stars*, He II + N V λλ4480–4760; *filled circles*, N V λ4944. *Right*: Simultaneous photometry, in magnitudes. *Open circles*, Strömgren *b* (dominance of He II λ4686); *filled circles*, Strömgren *y* (roughly continuum, tentatively adjusted to the *b* magnitudes by a simple zero-point shift, $\delta m = -1.080$ mag). Typical size of the 2 σ error bar is comparable to the symbol size in the RV panels, much smaller than the symbol size in the photometry panels, and runs at the level of 1% (the N V + He II complex) to 7% (O VI doublet) for the EW measurements.

motion in one out of three consecutive nights, which might explain the large scatter in the folded RV curve obtained from the 1993–1994 data (cf. Fig. 1 of Niemela, Barbá, & Shara 1995). Regarding the much higher amplitude of the RV variations from the 1993–1994 epoch compared with our data, we suggest (rather speculatively) the following: in 1993, the system was *probably* at a low flux state after the well-documented 1991–1992 maximum (Marchenko et al. 1998a, 1998b; Veen et al. 2000; however, the *Hipparcos* photometry was very sparse around 1993); however, the flux was rising again at the beginning of 1999 (Veen et al. 2000; A. Jones 1999, private communication). Thus, the long-term change of the RV amplitude may be linked to secular flux variations.

4. DISCUSSION

The presence of transient periodic RV variations seems to be undeniable. The more important question is, What lies behind this transient phenomenon? If it is a binary, then what could be the process that so efficiently but intermittently halts the RV variability induced by orbital motion? The abrupt ceasing of the RV variations might have a natural explanation if one were to assume a single, pulsating (or rotating) star. However, this assumption is

immediately contradicted by the finding that the *whole* O VI profile (out to $v = \pm 1500$ km s^{-1}) shifts during the $P = 0.329$ day cycle (Fig. 3*a*), while the line changes neither its equivalent width nor its FWHM (compare Figs. 3*a* and 3*b*), as would be expected for an emission component originating in any pulsating (or rotating) region of the inhomogeneous wind. From now on we will concentrate on the binary hypothesis as a more plausible explanation of the observed variability.

4.1. *Nature of the Emission Spectrum*

Before trying to find a reason behind the abnormal behavior of the O VI emission lines, we have to establish the nature of the emission spectrum of WR 46. The controversy stems from the conclusion reached by Steiner & Diaz (1998) that the system might belong to the group of "V Sagittae" variables, the newly established subclass of cataclysmic variables (CVs) with bright emission lines claimed to mainly originate in an accretion disk. On the contrary, model fitting of the WR 46 spectrum lends support to the status of WR 46 as a Population I W-R star (Schmutz et al. 1989; Hamann & Koesterke 1998), though with an abnormally strong O VI $\lambda\lambda$3811, 3834 doublet compared with the early-type WN stars of similar overall excitation (Crowther et al. 1995). Despite the typical W-R appearance of the WR 46 ultraviolet spectrum (strong P Cygni–like profiles of N V

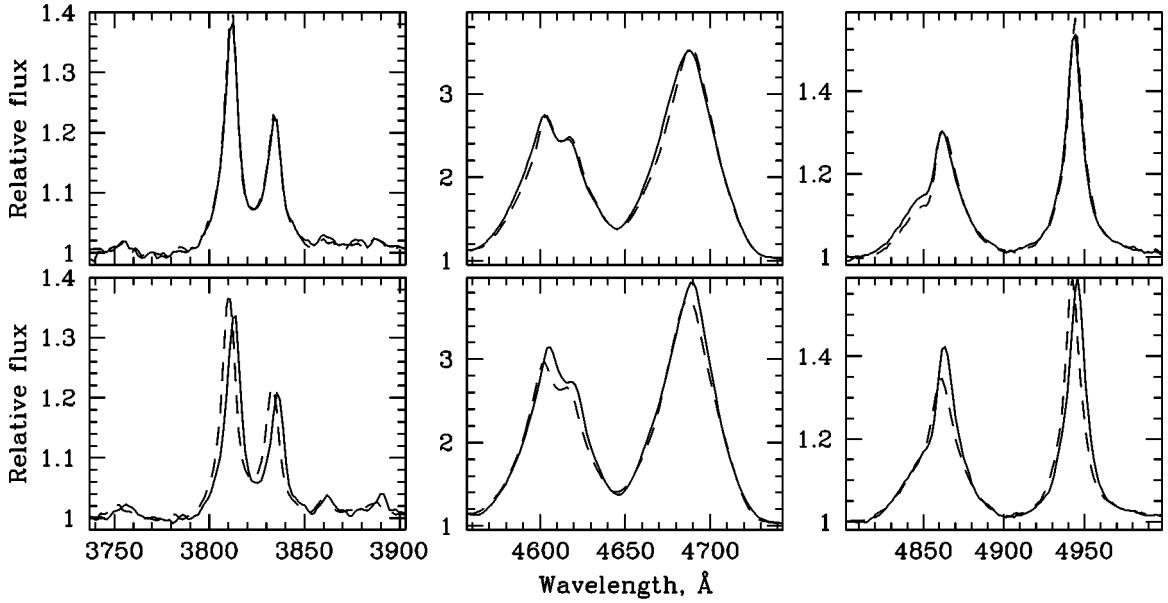

FIG. 3*a*

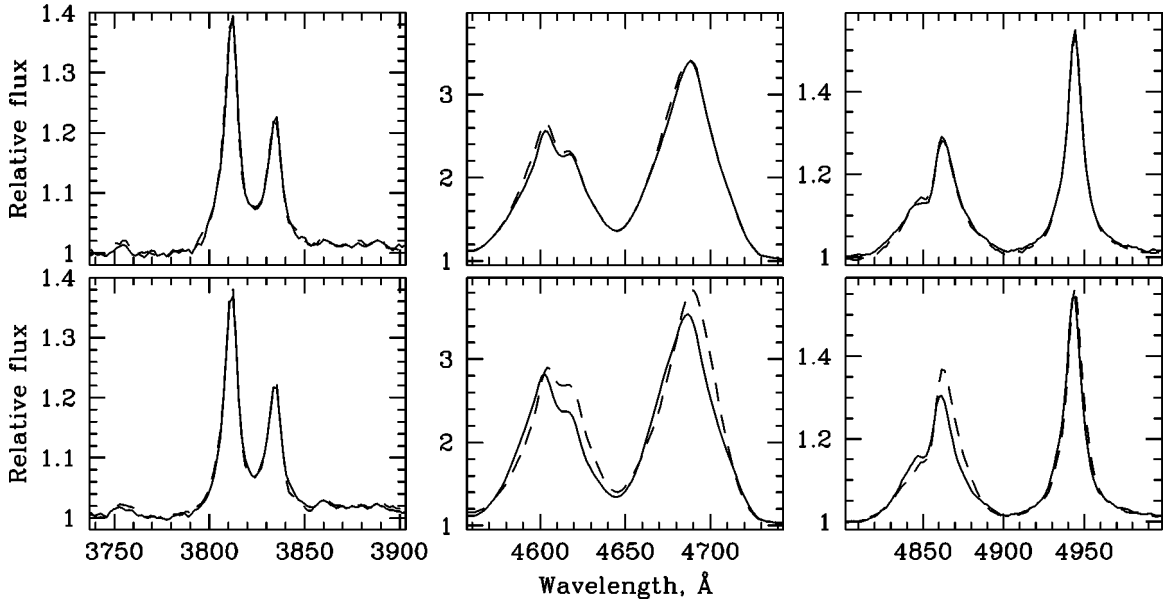

FIG. 3*b*

FIG. 3.—(*a*) *Top*, average of all available nonmoving spectra around $\phi = 0.0 \pm 0.05$ (*solid lines*) and the mean nonmoving spectrum for $\phi = 0.50 \pm 0.05$ (*dashed lines*); *bottom*, the same, but for the moving case. The phases were derived using $P = 0.329$ days, $T_0 =$ HJD 2,451,261.40 as tentative ephemeris. (*b*) Same as (*a*), but for phase $\phi = 0.25 \pm 0.05$ (*dashed lines*) vs. $\phi = 0.75 \pm 0.05$ (*solid lines*).

$\lambda\lambda$1238, 1242 and He II λ1640; Crowther et al. 1995), this argument cannot be used alone in support of a W-R origin for the WR 46 spectrum, as there are numerous CV systems with a similar mixture of absorption/emission details in their UV spectra (Córdova & Mason 1982, 1985). A more serious argument against the CV nature of WR 46 is the *complete* lack of hydrogen in its spectrum (Crowther et al. 1995; Hamann & Koesterke 1998; top panel of our Fig. 4, where the peak intensities of the He II Pickering lines do not show the odd-even "sawtooth" pattern expected in the presence of hydrogen—see also the numerous examples in Conti, Leep, & Perry 1983). The high effective temperature of WR 46 does not impair the detectability of hydrogen, as there are a few known examples of early-type WN stars with a substantial amount of hydrogen (Crowther et al. 1995; Smith, Shara, & Moffat 1996; Hamann & Koesterke 1998). On the other hand, a relatively small enhancement of He and/or CNO-cycle elements is present in the majority of CV systems (Warner 1995).

Moreover, the assumption, by direct analogy to a CV system, that reprocessing of X-ray and UV radiation in an accretion disk dictates formation of the emission-line optical spectrum of WR 46 also meets with strong objections. First, in WR 46 the strong stratification of the line formation zones (Fig. 4, *middle, bottom*) resembles the stratification of a typical W-R wind, where the lines of high ionization are narrowest, being formed in the inner, hotter wind at lower expansion velocity (Herald et al. 2000). This comes in sharp contrast to the dependence seen in the CV system IP Peg, where the emission profiles emerge from an accretion disk in Keplerian rotation (Marsh 1988). However, the straightforward interpretation of the spectral line morphology in WR 46 can be further complicated by the notion that in some CV systems the optical spectrum can be formed in a *wind* originating from the accretion disk (Murray & Chiang 1996).

Second, the WR 46 spectrum has an anomalously low line ratio of $r \equiv \mathrm{EW(H}\beta)/\mathrm{EW(He\ II\ }\lambda4686) < 0.1$, while $r \gtrsim 1$ in a typical CV system, with $r \gtrsim 0.3$ for the most extreme cases (Patterson & Raymond 1985a). The low value of the observed X-ray flux (Pollock, Haberl, & Corcoran 1995), being related to the estimated absolute magnitude of WR 46 (Crowther et al. 1995), provides indirect evidence that the accretion rate should not be less than $\dot{M} \sim 10^{17}$–10^{18} g s^{-1} [$1.6 \times (10^{-9}$ to $10^{-8})\ M_\odot$ yr^{-1}] if one places WR 46 on the diagnostic diagrams developed for CV systems (Patterson & Raymond 1985a). For CV systems, this means that He II λ4686 emission could be formed mainly via reprocessing of radiation in an optically thick accretion disk, producing EW(He II λ4686) $\lesssim 10$ Å (Patterson & Raymond 1985b). However, we observe a far stronger EW(He II λ4686) $\gtrsim 100$ Å in WR 46. Hence, the bulk of the He II emission flux in WR 46 must originate in a W-R wind, with some supplement (see below) from a highly variable emission component produced in the vicinity of the unseen companion. Noteworthy is that the general shapes of the emission profiles of WR 46 resemble those observed in the presumably single (Marchenko et al. 2000) WN3 star WR 3 (Fig. 5), apart from the strong wind-formed He II absorptions of WR 3. On the other hand, the general morphology of WR 46's spectrum differs from that of an average "supersoft source" (SSS) spectrum (Cowley et al. 1998; note that the "V Sagittae" variables could be a subclass of the SSS binaries; Steiner & Diaz 1998). For example: (1) The EW ratio of Hβ to He II λ4686 is $\sim$0.3 in SSSs, while it is $\sim$0.1 for WR 46. (2) There is a clear presence of hydrogen in the emission spectra of SSSs, while none is detected in WR 46. (3) The O VI $\lambda\lambda$3811, 3834 doublet has approximately the same strength in all SSS

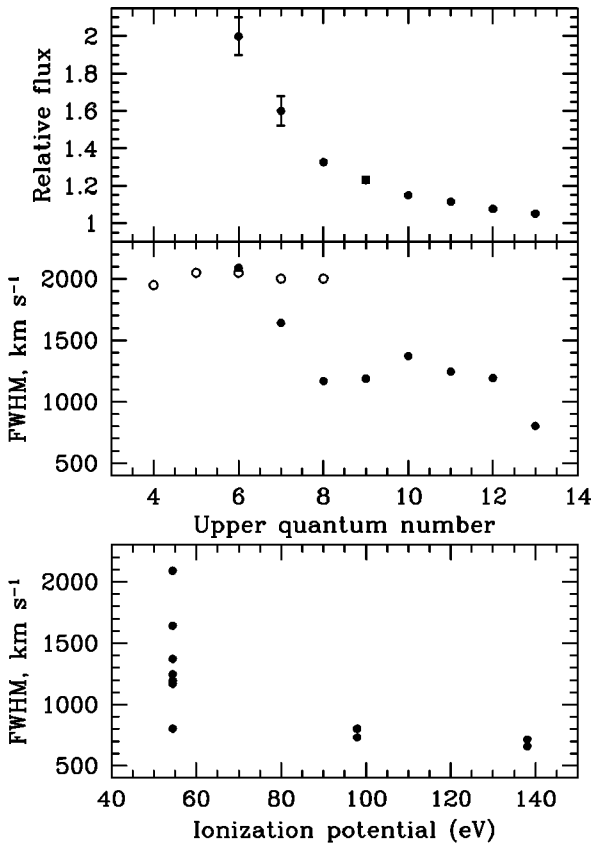

FIG. 4.—*Top*, peak intensities of the He II Pickering lines in the average rectified spectrum of WR 46 with corresponding 2 σ error bars; *middle*, the FWHM values for the Balmer lines in the CV IP Peg (*open circles*) and the FWHM for the He II Pickering lines in WR 46 (*filled circles*); *bottom*, FWHM for lines of different ionization potential in WR 46.

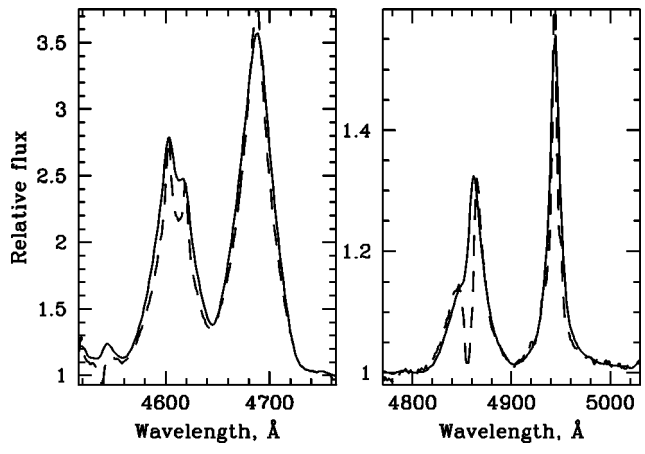

FIG. 5.—Average spectrum of WR 46 (*solid lines*) compared with the averaged WR 3 spectrum (*dashed lines*). The initially higher resolution WR 3 spectrum was convolved with a Gaussian instrumental profile corresponding to the configuration used for WR 46. In addition, the WR 3 spectrum was multiplied by a constant value (2.03) to match the intensities of the WR 46 profiles.

spectra, while it is at least a factor of 3 stronger in WR 46. (4) The width of the He II 4686 Å line in WR 46, FWHM = 16.5 Å, is significantly larger than the corresponding width in the SSS spectra, $\langle \mathrm{FWHM} \rangle = 7.8 \pm 3.1$ Å.

Third, in WR 46 the magnitude of line profile and RV variations peaks around the line centers, rapidly decreasing toward the line wings (see below), contrary to the high activity of the emission-line wings in CV systems.

Even if one were to assume that the emission spectrum of WR 46 is formed in an accretion disk in a hydrogen-deficient binary system, then at least two outstanding problems posed by the W-R scenario would still remain unsolved: (1) how to explain the peculiar overabundance of oxygen and the lack of carbon features (note that the remaining three V Sagittae–like stars show the presence of C III λ4650 emission; Steiner & Diaz 1998); (2) why do the O VI lines suddenly stop showing signs of orbital motion?

4.2. *Temporal Spectral Variability*

Having established that a W-R wind is likely to be the principal component of the emission spectrum in WR 46, we may now turn to the still unsolved puzzle of the RV variations. For the sake of argument, let us assume that the apparent intermittent "ceasing" of the orbital motion is rooted in a sudden change of the wind structure. As a possible consequence, the visible size of the W-R component would change too, being controlled by the opacity of the W-R continuum, which could ultimately lead to engulfing of the closely orbiting companion and diminishing of the RV amplitude. Following this assumption, one can check for a substantial difference in the general appearance of the moving and nonmoving spectra. Constructing a mean "nonmoving" spectrum from all available night 1, 2, and 5 spectra (58 in total), we promptly find that it does not deviate from the "moving" mean (the 76 spectra from nights 3, 4, 6, and 7 Doppler-corrected for the source's motion) in a way that supports our expectations about radical change in the wind structure. Comparing the moving and nonmoving mean spectra (Fig. 6), one can deduce that, aside from the variable central parts of the profiles, there is little change in the overall shape of the emission lines and, possibly more important, in the relative strengths of the diagnostic emission features, e.g., EW(N V λ4944) versus EW(N V + He II) in Figure 7. Neither the wind's velocity structure nor the ionization structure of the outer wind seems to vary to a sufficient degree to explain the switch between the nonmoving and moving cases.

The relatively small changes in the overall appearance of the spectra seen in Figure 6 have a fairly simple explanation. By coincidence, the moving spectra happened to have been taken preferentially around the system's high state (nights 3, 4; cf. Fig. 2, *right*), thus sampling a slightly cooler, somewhat "puffed up" wind, with growing emissivity in the lines of relatively low ionization/excitation potential (Fig. 7). Indeed, relatively small temperature variations, $\Delta T < 1000$ K, were deduced from observed color variations in WR 46 (Schmutz 1991). Qualitatively, we can confirm this conclusion when inspecting the available *UBVRI* data, where some color changes are noticeable only for the extreme cases, i.e., in the plots of *U* versus *V* or *U* versus *I* (Fig. 8). They follow the well-established general trend (Veen et al. 2000), with the higher flux state of the system corresponding to a lower temperature. Thus, we may safely conclude that the relatively small differences in the appearance of the moving and nonmoving spectra have nothing to do with the expected radical changes in the ionization/velocity structure of the W-R wind. The only, though rather indirect, evidence for a changing W-R wind opacity comes from Figure 1 (*top*), where one can see a large, ~ 50 km s^{-1}, systemic velocity shift in the RV variations from nights 3 and 4 ("moving" high state) compared with nights 6 and 7 ("moving" low state). We point to the intriguing resemblance of this phenomenon to the changing systemic velocity of the eruptive W-R + OB binary HD 5980 (Fig. 3 of Moffat et al. 1998). In both systems, the systemic RV changes are accompanied by substantial growth of the EW of He II lines. In WR 46, the growth of continuum flux during the high state of the system could lead to growth of the sizes of the line formation zones and, at the same time, to enhancement of the line's self-absorption, thus creating the slightly redshifted (O VI doublet) or significantly skewed (He II lines) profiles.

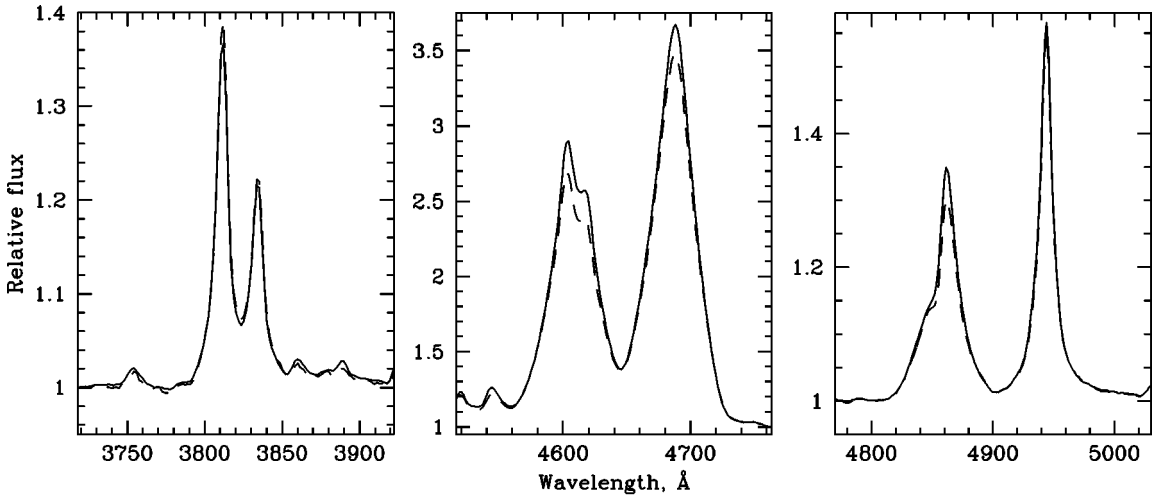

FIG. 6.—Mean nonmoving spectrum, a direct combination of 58 spectra from nights 1, 2, and 5 (*dashed lines*), and the mean moving spectrum produced via combination of the 76 Doppler-corrected spectra from nights 3, 4, 6, and 7 (*solid lines*). Doppler correction of each spectrum into the source's rest frame was performed using the binned RV curve (Fig. 1, *top*). In each panel, the wavelength interval roughly corresponds to 1.6×10^4 km s^{-1}. Note the difference in the intensity scales.

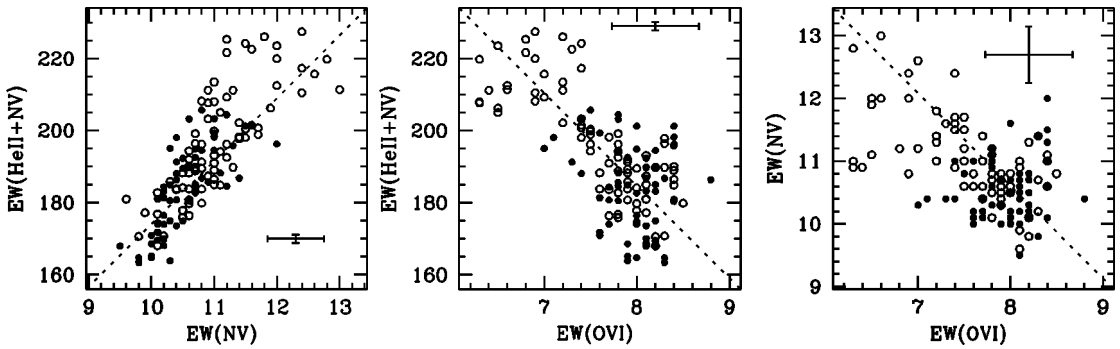

FIG. 7.—Variability in EW of the prominent emission features. Open circles denote the measurements in the moving spectra; filled circles correspond to the nonmoving case. Dotted lines denote a perfect correlation (anticorrelation) and are plotted for guidance only. The 2 σ error bars (calculated as in Chalabaev & Maillard 1983) are shown.

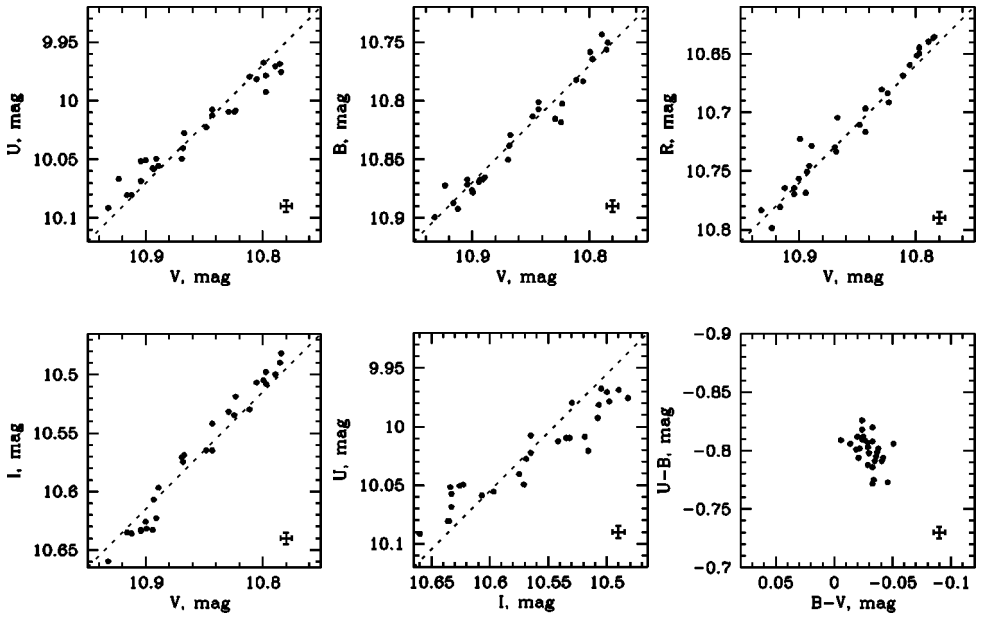

FIG. 8.—The *UBVRI* photometry of WR 46 with 2 σ error bars. Dotted lines correspond to a 1 : 1 correlation and are plotted for guidance only.

Is there any significant dissimilarity in the variability patterns of the moving and nonmoving sets of spectra? One way to assess the line profile variability is to evaluate its temporal variance spectrum (TVS; Fullerton, Gies, & Bolton 1996) for each night and compare the results. In so doing, we calculated a slightly modified (Marchenko et al. 1998a) version of the TVS. In Figure 9, we show the rescaled TVS along with the mean WR 46 spectrum. The rescaled TVS was obtained from the original one by taking the square root of the initial TVS and then dividing this by the corresponding mean spectrum, thus providing the possibility to compare variations in the profiles of different intensity. Apparently, there are some differences in the structure of the moving and nonmoving TVSs, namely, the TVS intensity is significantly higher in the moving subset. As we will show below, the magnitude of the line profile variability depends on the level of the continuum flux, with higher flux corresponding to a higher level of line variability. Hence, the higher amplitude of the moving TVS could be linked to the fact that the moving spectra were preferentially taken during the high flux state of the system. Also, the moving TVS is more structured, thus reflecting the variability

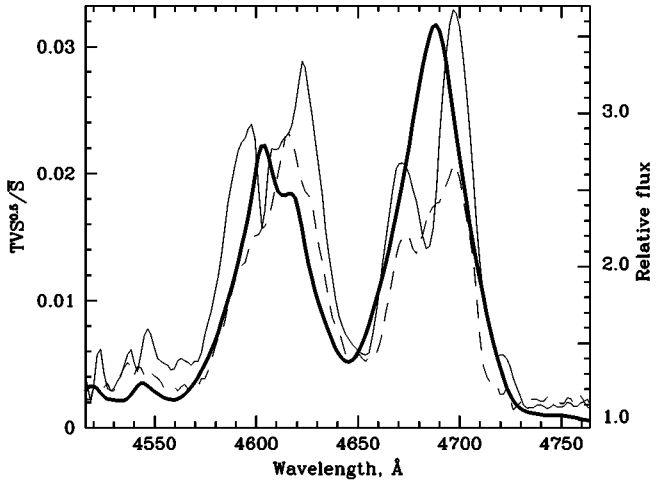

FIG. 9.—Comparison of the rescaled TVSs. *Thin solid line*, average of TVSs from nights 3, 4, 6, and 7, i.e., the moving case; *dashed line*, average nonmoving TVS for nights 1, 2, and 5; *thick line*, mean WR 46 spectrum.

pattern prevailing in the moving spectra, i.e., the velocity shifts of the uppermost portions of the emission profiles in the lines of a relatively low ionization and/or excitation potential, namely, He II λ4686 and N V $\lambda\lambda$4603, 4619 (Fig. 3). In both the moving and the nonmoving TVS, we observe a rapid falloff of the TVS amplitude toward the line wings, clearly pointing to a concentration of activity around the line cores.

The traditional TVS approach does not tell much about the temporal behavior of the variability patterns, unless the amount of data is sufficient to allow one to estimate a TVS on short time intervals. This is clearly not the case for WR 46. To explore the short-term variability of WR 46, we developed a special technique, which resembles a simple cross-correlation approach, however with the ability to deal with unequally sampled data. First, we produce the normalized differences for all available spectra taken within one night:

$$\Delta J(\Delta t_{ij}, \lambda) = \tfrac{1}{2}[I(t_i, \lambda) - I(t_j, \lambda)]/[I(t_i, \lambda) + I(t_j, \lambda)], \quad (1)$$

where $I(t_i, \lambda)$ represents the wavelength-dependent flux in the spectrum taken at time t_i. Then, for the given Δt_{ij} all the $\Delta J(\Delta t_{ij})$ differences are averaged within sufficiently broad wavelength intervals, typically $(0.1–0.5)I_{max}$ and $(0.5–1.0)I_{max}$ for the blue and the red side of the profile, correspondingly. The last operation is to average the $\Delta J(\Delta t_{ij}, \bar{\lambda})$ differences falling into the given time interval, $\Delta t_l = t_l$ to $t_l + \delta t$. For the sake of simplicity, we choose $t_l = l\,\delta t$, with $l = 0, \ldots, N-1$ and $\delta t = (\max\{\Delta t_{ij}\} - \min\{\Delta t_{ij}\})/(N-1)$, where N is the total number of spectra for the given night, $i = 1, \ldots, N$, and $j = 1, \ldots, N$. To estimate the significance of the observed variability, we plot in Figure 10 the normalized $\Delta J(\Delta t_l, \bar{\lambda})$ differences together with the adequately obtained values for the nearby continuum. For a typical S/N > 200 spectrum, the observational errors are dominated by the uncertainty of the continuum placement. This approach can provide a wide variety of diagnostic diagrams. Apparently, in the case of clearly periodic line profile variations the $\Delta J(\Delta t_l, \bar{\lambda})$ values in each analyzed line should also oscillate with the given period, provided there are coherent variations across the profile of the given line as well as line-to-line compatibility.

However, this fairly simple case seems never to be at work in WR 46. The first, quite straightforward conclusion is that, with rare exceptions, the variability is confined to the central parts of the line profiles, $(0.5–1.0)I_{max}$ in our definition. A less encouraging result is that there are no distinguishing features in the variability patterns of the moving and nonmoving spectra, with the exception of the O VI 3811 Å line (we have measured only one component of the doublet), where one sees no significant variations in the nonmoving data series but the moving data show a clear anticorrelated activity in the central parts of the profile. The latter has a trivial explanation, if one considers the back-and-forth motion of the line during the moving phases. Indeed, in the two fixed wavelength intervals [e.g., the blue and red sides of the emission profile, $(0.5–1.0)I_{max}$] the orbital motion should produce deviations of opposite sign from a mean profile if (1) the time lags are close to half of the orbital period and (2) the orbital RV amplitude is smaller than the line half-width. The variability patterns of the O VI λ3811 profile practically never resemble those in the rest of the simultaneously observed prominent emission profiles. The $(0.5–1.0)I_{max}$ red side of the N V λ4944 profile fares slightly better, sometimes approximately following the He II line variability. In general, there are fairly compatible patterns in the variability of the He II 4686 Å and 4860 Å lines, with the red parts of the profiles moving more coherently than the blue parts. However, the correlation is frequently broken between the upper red, $(0.5–1.0)I_{max}$, and upper blue parts of a given line, which proves that local, irregular perturbations sometimes prevail in the variability patterns. Generally, there is a superposition of long-term trends and pulsational patterns. For one out of three "nonmoving" nights, we detected a pulsation-like pattern in the He II line (Fig. 10), suggestive of ongoing periodic activity.

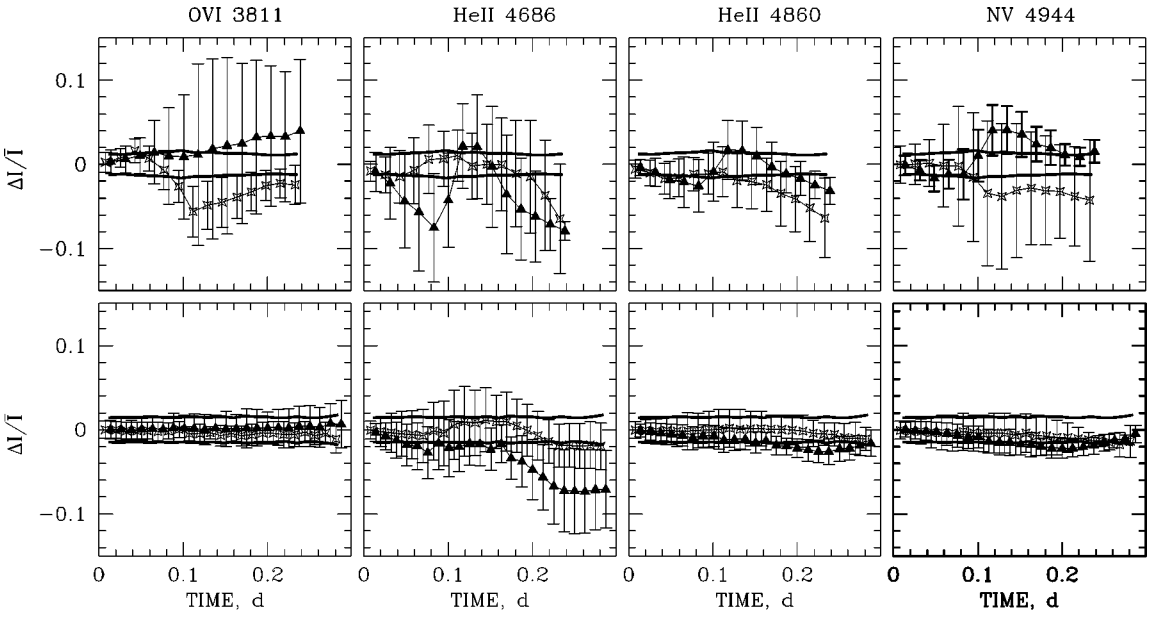

FIG. 10.—*Top*, time dependence of perturbations for the most prominent emission lines in the night 3 spectra (moving case); *bottom*, night 5 spectra (nonmoving case). Stars denote the averaged differences for the center-to-blue (from I_{max} to $\sim 0.5I_{max}$) parts of the profiles; triangles mark the averages for the center-to-red parts (from $\sim 0.5I_{max}$ to I_{max}). The horizontal lines denote a 95% detectability limit.

4.3. *High- and Low-State Spectral Transformations*

Now we examine the high-flux and low-flux transitions of the system in more detail, as those changes may shed some light on the nature of the unseen companion. To reveal the dependence of the flux emerging from prominent emission lines on the level of the continuum flux, we preselect all the EW measurements that are accompanied by practically simultaneous ($\delta t < 0.01$ days) photometric observations, using linear interpolation for the overlapping photometry if necessary. We plot the corresponding dependencies in Figure 11, confirming the suspicion (see Figs. 1 and 7) that the flux of the O VI doublet hardly varies at all, while the *apparent* O VI variability is caused by the variable continuum level. On the contrary, the fluxes of the N V λ4944 and He II λ4686 + N V $\lambda\lambda$4603, 4619 emissions increase in proportion to the rising $f^2_{\rm cont}$ values, where $f_{\rm cont}$ is the continuum flux. However, the proportionality is lost when the continuum flux drops below a critical level. Rather unexpectedly, we find a reasonably good match to the He II + N V behavior by applying the $\log L$(He II λ4686)–$\log \dot{M}_{\rm accr}$ dependence for CVs from Patterson & Raymond (1985b) with a rescaling (by a factor of 30) of $\log L$(He II λ4686) and substitution of $\log \dot{M}_{\rm accr}$ by y with an appropriate zero-point shift (Fig. 11). The original $\log L$(He II λ4686)–$\log \dot{M}_{\rm accr}$ dependence was calculated for the CV systems, for which all the He II λ4686 line emissivity is produced in the accretion disk via reprocessing of soft X-ray radiation. In WR 46, the observed *change* in the He II λ4686 line emissivity (i.e., the extra flux generated in the line core, excluding the relatively quiet "base" of the line) closely follows the reprocessed radiation dependence, so it is tempting to conclude that this *extra* emissivity is generated by a similar mechanism. Indeed, one may assume that the initial rise in the continuum flux level (whatever the cause of the rise) leads to some increase in the wind mass-loss rate, $\dot{M}_{\rm wind}$, from the W-R component and, proportionally, to the increment in the accretion rate, $\dot{M}_{\rm accr}$, thus driving up the reprocessed flux and, as a consequence, the wind-plus-disk emissivity.

One can be assured that at least the $\dot{M}_{\rm wind}$ channel works in WR 46: the high-flux to low-flux transition affects the profiles *globally*, i.e., involving both the blue and the red parts of the profiles, however with greater impact on the regions corresponding to an "instantaneous" (in velocity space, for a given orbital phase) position of the W-R component (see Fig. 12 and below). The profound line profile changes are accompanied by perceivable color variations (Fig. 8). The less prominent Pickering He II lines closely follow the behavior of He II λ4686 (Fig. 12). Again, we point to the fact that we observe relatively small temperature variations during large changes of the continuum flux: the relative amplitudes of the line profile variations quickly diminish in the Pickering He II lines and N V lines of higher excitation potential; the same is true if one considers the difference in the ionization potentials of the O VI, N V, and He II lines (Fig. 12). One detail provides indirect evidence that the $\dot{M}_{\rm accr}$ channel might be in active operation along with the traditional $\dot{M}_{\rm wind}$ mechanism, thus producing some extra line and continuum emissivity via the reprocessing of radiation emitted by an accretion disk. In CV systems, there is a good correlation between the luminosity of the

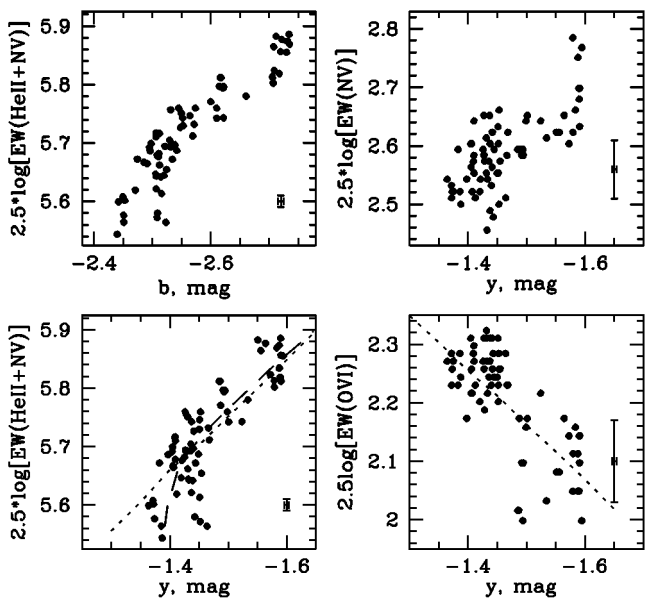

FIG. 11.—Available b, y photometry and simultaneously measured EWs with corresponding 2 σ error bars. The dotted line in the O VI vs. y panel marks the predicted behavior of the line flux in the case when a line of constant flux is placed on a variable continuum. The dotted line for the He II + N V vs. y dependence shows the case in which the line flux grows in proportion to $f^2_{\rm cont}$. In the same panel the dashed line follows the scaled-down trend for reprocessed emission (see text).

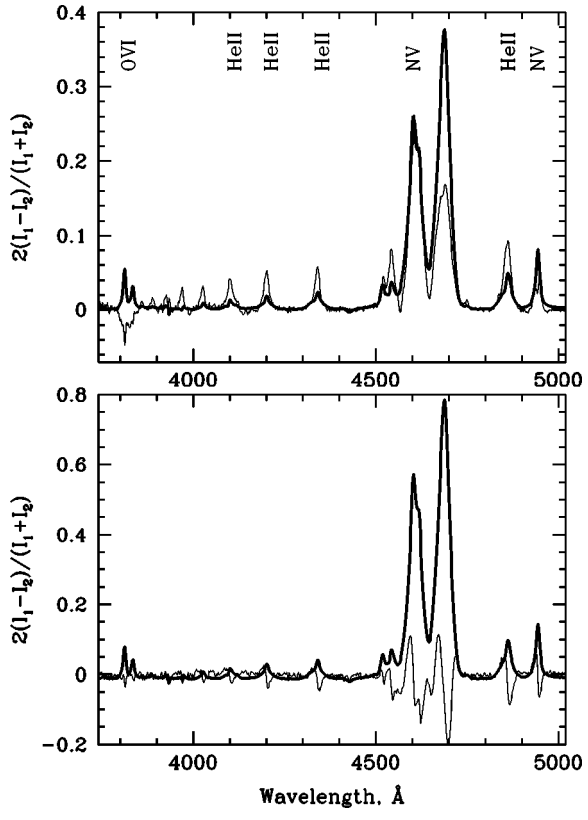

FIG. 12.—*Top*, normalized difference between the high-flux and the low-flux states of the system (*thin line*), where I_1 corresponds to the mean night 4 spectrum and I_2 is the mean night 2 spectrum, and the average spectrum from nights 2 and 4 (*thick line*); *bottom*, the same normalized difference, but with I_1 as a mean of three spectra taken around $\phi = 0.75 \pm 0.05$ on night 4 and I_2 as a mean of three spectra corresponding to $\phi = 0.25 \pm 0.05$ on the same night, with the thick line depicting the average night 4 spectrum.

"constant" part of the system's flux (a combination of the fluxes from the white dwarf and accretion disk) and the luminosity of the flickering source, suggestive of the flickering's being powered in some way by the accretion disk (Bruch 1992). In terms more appropriate for WR 46, we ask, Is there any correlation between the system's continuum flux and the level of line variability? Integrating the normalized, nightly averaged TVS (see above) along the line profiles, additionally rescaling them by their seven-night average values and plotting them versus the nightly averaged continuum flux (Fig. 13), we encounter the expected trend: the source activity increases with the rising continuum flux level.

The discovered short-term (hours, days) trends in variability of the He II emission-line fluxes fall in line with the long-term (months, years) correlation between the continuum flux and the EW of the He II 5412 Å line (Veen et al. 1995; Veen, van Genderen, & Jones 1999; Veen et al. 2000). This lends additional support to the suggestion that the unusually high activity of the WR 46 system is driven by the low/high flux transitions in the W-R core, with the close-orbit companion as a possible cause of the transitions.

4.4. *Nature of the Unseen Companion*

Concerning the nature of the unseen companion, we note the resemblance (within the "noise") of the WR 46 light curve (Fig. 1) to the V-shaped light curves produced by atmospheric eclipses in well-known W-R + O binaries (Lamontagne et al. 1996). The light-curve minimum in WR 46 occurs close to the time of passage of the emission-line source (presumably a normal W-R star) in front of the companion, as for a typical W-R + O system. However, we have no intention of overinterpreting this nice coincidence. So far, the system has produced a wide variety of light curves, which, for a majority of cases, showed an incoherent structure when phased with $P = 0.329$ days (P. M. Veen 2000, private communication; see also Veen et al. 2000). Moreover, some of the abundant photometric data discussed by Veen et al. may be folded with alternating periods, e.g., 0.2727 and 0.2825 days, to yield coherent structure. Unfortunately, our second subset of photometry (Table 2) provides too sparse a phase coverage on a background of high-amplitude erratic variability, thus making any meaningful conclusions about stability of the light-curve shape virtually impossible. Apparently, the nature/nurture of the remarkable WR 46 variability cannot be clarified when judging solely by the forms of "snapshot" light curves.

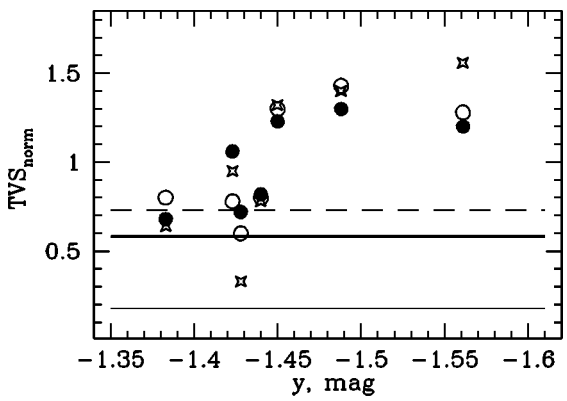

FIG. 13.—Dependence of the line-integrated, rescaled TVS on the nightly averaged continuum flux. *Open circles*, the O VI doublet; *stars*, the He II + N V complex; *filled circles*, the N V λ4944 profile. Dashed, thick, and thin solid lines provide the 95% detectability levels for the aforementioned lines, respectively.

The primary minima in the EWs of He II and N V around $\phi = 0.75$, as well as the much shallower (allowing for the variable continuum level) dips at $\phi \sim 0.25$ (Fig. 1, *bottom*), are more informative. One may conclude that some emissivity in the lines of a relatively (to O VI) low ionization potential might come from the unseen companion (minimum at $\phi = 0.25$), thus supporting the earlier suggestion about the reprocessed nature of the *extra* emissivity seen in the He II + N V complex. There is a possible small phase shift between the phase dependencies of EW(N V λ4944) and EW(He II + N V), which seemingly increases with rising continuum level (compare night 2 with night 4 in Fig. 2, *middle*) and highlights a potential asymmetry of the emissivity region. Analysis of the phase-dependent profile variability in the individual spectra also points to the asymmetric shape of the emissivity zone. Clearly, during maximum light there is an extra emission component forming in all the He II lines and in the N V λλ4603, 4619 lines and even, to a lesser extent, in the N V λ4944 feature (Fig. 12, *top*). However, this component is distributed quite asymmetrically, as can be readily deduced from the large phase lags in the RV variations of the O VI and He II + N V emissions (Fig. 2, *left*). Plotting the normalized difference between the average $\phi = 0.75 \pm 0.05$ and average $\phi = 0.25 \pm 0.05$ profiles from night 4 in Figure 12 (*bottom*), we find that the extra emission component is shifted to the blue side of the profile at $\phi = 0.75$, moving to the red side at $\phi = 0.25$ (compare with Fig. 3*b*). The asymmetry created by the presence of the extra emission is much less pronounced during the low flux state of the system. This phase-dependent positioning of the relatively (to the total line widths) broad additional emission suggests that it must be formed in part of the W-R wind. Then, passing in front of the system at $\phi \sim 0.75$, this extra emissivity zone of presumably higher optical density could account for the observed enhanced P Cygni absorption components in the He II Pickering lines along with some reduction of the equivalent widths and continuum flux (Figs. 1, 12) due to an atmospheric eclipse (cf. Auer & Koenigsberger 1994 and references therein). One can readily see the enhancement of the P Cygni absorption in Figure 14, where we plot the bisectors of prominent emission lines: note the rapid change of the velocity corresponding to the ~0.4 intensity level in the He II λ4859 profile taken at $\phi \sim 0.75$ (Fig. 14, *top*). Also note the sloped bisectors of the He II 4686 Å line, which point to significant self-absorption in the wind.

The emission flux from the W-R component seems to dominate the optical spectrum of WR 46. We also deduced, though only indirectly, that there might be some output from the unseen companion too. Can the optical emission from the unseen companion be formed in a putative accretion disk? Assuming orbital motion of the W-R component with $K \sim 90$ km s^{-1} (Fig. 1, *top*), one obtains the mass of the unseen companion, $M_c \sim 1.4\ M_\odot$—as for a "classical" neutron star, for an $i = 90°$ orbit and a typical W-R star of $M_{WR} = 10\ M_\odot$. Using the approach developed by Wang (1981), we find that in WR 46 an accretion disk can be formed around a putative neutron star, thanks to the extremely short orbital period and small size of the neutron star, despite the very high relative velocity of the accreted

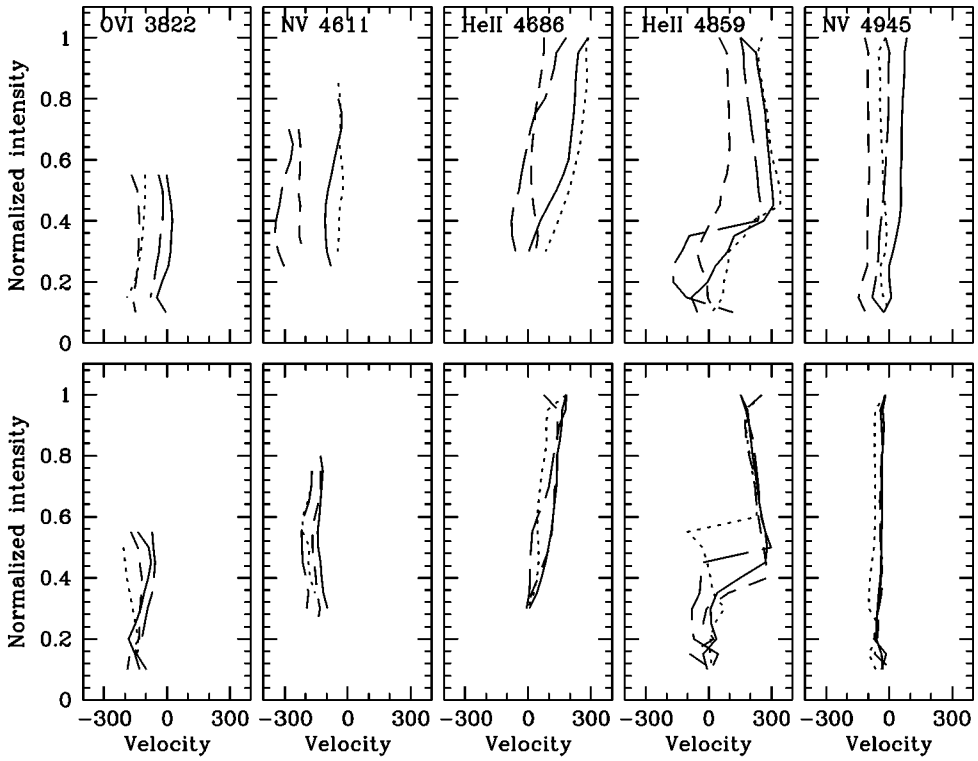

FIG. 14.—Bisectors of prominent emission lines calculated for the $I_{min}, \ldots, fI_{max}$ line intensity ranges and in $0.05I_{max}$ steps, where I_{max} is a maximum line intensity; I_{min} and f are chosen to avoid blending problems. The bisectors were calculated for the individual spectra (*top*, night 3, moving case; *bottom*, night 2, nonmoving case) taken $\Delta\phi \sim 0.25$ apart. The solid lines denote the bisector for $\phi \sim 0.0$, the dotted lines mark the bisector for $\phi \sim 0.25$, the short-dashed lines mark the bisector for $\phi \sim 0.5$, and the long-dashed lines denote the bisector for $\phi \sim 0.75$.

matter, $v_{rel} = (v_{orb}^2 + v_{wind}^2)^{0.5} \sim 10^3$ km s^{-1}, where $v_{orb} \leq 0.5 \times 10^3$ km s^{-1} is the orbital velocity of the companion and $v_{wind} \geq 0.7 \times 10^3$ km s^{-1} (Marchenko & Moffat 1999) is the minimal W-R wind velocity at $r = a$ (orbital separation). The presence of an optically thick ($\dot{M} > 10^{16}$ g s^{-1}; see Patterson & Raymond 1985b and above) accretion disk can explain the low X-ray luminosity of WR 46 (Pollock et al. 1995). On the other hand, the high relative velocity makes formation of an accretion disk unlikely if the companion is an early-type main-sequence star or even a white dwarf.

5. CONCLUSIONS

Analysis of our new, abundant, high-quality spectroscopic and photometric data on the suspected binary WR 46 reveals a complicated superposition of seemingly random, relatively long-term variability and a clearly periodic, coherent component with $P = 0.329 \pm 0.013$ days. Amplitudes of the former process frequently dominate the latter in equivalent width fluctuations and almost completely suppress any periodic variations in photometry (representing the continuum flux). However, the periodic signal, which can be reconciled with orbital motion of the W-R component, wins over the stochastic component from time to time in the radial velocity measurements. In an attempt to solve the puzzle of the intermittently disappearing, periodic RV variations, we find only indirect evidence for a changing physical size of the W-R wind in the form of epoch dependency of the systemic velocity. We conclude that the optical spectrum of WR 46 is dominated by the emission lines formed in the wind of a Population I W-R star, with some relatively minor contribution coming from reprocessed radiation in the vicinity of an unseen companion. The unusually high activity of the binary is governed by rapid (hours to days) transitions between high and low states of the system's continuum flux. It remains to be seen whether the presence of a closely orbiting component can be responsible for (1) the system's unusually high activity and (2) the peculiar chemical composition (cf. Crowther et al. 1995) of the W-R component. Also, it should be clarified to what extent the morphology of the observed line profile variations depends on the long-term (years; cf. Veen et al. 2000) changes of the system's flux, as we have for now only a few observations that imply such a dependence, in particular, the aforementioned difference in the RV amplitude deduced from the 1993 and 1999 data sets. On the other hand, the mysterious, abrupt ceasing of the periodic RV variations seems to be impervious to the high/low flux transitions in the system.

We thank the director and staff of CASLEO for the use of their facilities. We acknowledge the use at CASLEO of the CCD and data acquisition system supported under NSF grant AST 90-15827 to R. M. Rich. A. F. J. M. and S. V. M. wish to thank the National Science and Engineering Research Council of Canada and FCAR of Quebec for continuing financial support. C. S. thanks Torben Arentoft for his help in the reduction of the CCD frames. Financial support from the Belgian Fund for Scientific Research is acknowledged. This project was partly supported by the Flemish Ministry for Foreign Policy, European Affairs, Science, and Technology.

REFERENCES

Auer, L. H., & Koenigsberger, G. 1994, ApJ, 436, 859
Bruch, A. 1992, A&A, 266, 237
Chalabaev, A., & Maillard, J.-P. 1983, A&A, 127, 279
Conti, P. S., Leep, E. M., & Perry, D. N. 1983, ApJ, 268, 228
Córdova, F. P., & Mason, K. O. 1982, ApJ, 260, 716
———. 1985, ApJ, 290, 671
Cowley, A. P., Schmidtke, P. C., Crampton, D., & Hutchings, J. B. 1998, ApJ, 504, 854
Crowther, P. A., Smith, L. J., & Hillier, D. J. 1995, A&A, 302, 457
Fullerton, A. W., Gies, D. R., & Bolton, C. T. 1996, ApJS, 103, 475
Hamann, W.-R., & Koesterke, L. 1998, A&A, 333, 251
Herald, J. E., Schulte-Ladbeck, R. E., Eenens, P. R. J., & Morris, P. 2000, ApJS, 126, 469
Kingsburgh, R. L., & Barlow, M. J. 1995, A&A, 295, 171
Lamontagne, R., Moffat, A. F. J., Drissen, L., Robert, C., & Matthews, J. M. 1996, AJ, 112, 2227
Marchenko, S. V., et al. 2000, in preparation
Marchenko, S. V., & Moffat, A. F. J. 1999, A&A, 341, 211
Marchenko, S. V., Moffat, A. F. J., Eversberg, T., Hill, G. M., Tovmassian, G. H., Morel, T., & Seggewiss, W. 1998a, MNRAS, 294, 642
Marchenko, S. V., et al. 1998b, A&A, 331, 1022
Marsh, T. R. 1988, MNRAS, 231, 1117
Moffat, A. F. J., et al. 1998, ApJ, 497, 896
Murray, N., & Chiang, J. 1996, Nature, 382, 789
Niemela, V. S., Barbá, R. H., & Shara, M. M. 1995, in IAU Symp. 163, Wolf-Rayet Stars: Binaries, Colliding Winds, Evolution, ed. K. A. van der Hucht & P. M. Williams (Dordrecht: Kluwer), 245
Patterson, J., & Raymond, J. C. 1985a, ApJ, 292, 535
———. 1985b, ApJ, 292, 550
Pollock, A. M. T., Haberl, F., & Corcoran, M. F. 1995, in IAU Symp. 163, Wolf-Rayet Stars: Binaries, Colliding Winds, Evolution, ed. K. A. van der Hucht & P. M. Williams (Dordrecht: Kluwer), 512
Roberts, D. H., Lehár, J., & Dreher, J. W. 1987, AJ, 93, 968
Schmutz, W. 1991, in IAU Symp. 143, Wolf-Rayet Stars and Interrelations with Other Massive Stars in Galaxies, ed. K. A. van der Hucht & B. Hidayat (Dordrecht: Kluwer), 39
Schmutz, W., Hamann, W.-R., & Wessolowski, U. 1989, A&A, 210, 236
Smith, L. F., Shara, M. M., & Moffat, A. F. J. 1996, MNRAS, 281, 163
Steiner, J. E., & Diaz, M. P. 1998, PASP, 110, 276
van der Hucht, K. A., Conti, P. S., Lundström, I., & Stenholm, B. 1981, Space Sci. Rev, 28, 227
Veen, P. M., van Genderen, A. M., & Jones, A. F. 1999, in IAU Symp. 193, Wolf-Rayet Phenomena in Massive Stars and Starburst Galaxies, ed. K. A. van der Hucht, G. Koenigsberger, & P. R. J. Eenens (San Francisco: ASP), 263
Veen, P. M., van Genderen, A. M., van der Hucht, K. A., Arentoft, T., & Allen, B. 2000, A&A, submitted
Veen, P. M., van Genderen, A. M., Verheijen, M. A. W., & van der Hucht, K. A. 1995, in IAU Symp. 163, Wolf-Rayet Stars: Binaries, Colliding Winds, Evolution, ed. K. A. van der Hucht & P. M. Williams (Dordrecht: Kluwer), 243
Wang, Y.-M. 1981, A&A, 102, 36
Warner, B. 1995, Cataclysmic Variable Stars (Cambridge: Cambridge Univ. Press)